Secondary Atomization of Newtonian Liquids in the Bag Breakup Regime: Comparison of Model Predictions to Experimental Data

V. Kulkarni, D.R. Guildenbecher†, P.E. Sojka*

Maurice J. Zucrow Laboratories,
School of Mechanical Engineering,
Purdue University, West Lafayette, IN, U.S.A.

vkulkarn@purdue.edu , drguild@sandia.gov, sojka@ecn.purdue.edu

Abstract

Secondary atomization refers to the fragmentation of liquid drops due to aerodynamic forces exerted by a surrounding gas-phase. It is important in the context of combustion applications as improved understanding of the underlying physical phenomena can lead to better engine efficiencies. In the current work we examine one aspect of the secondary atomization process i.e., the deformation of an inviscid drop when exposed suddenly to a flowing air stream. The bag breakup mode is one such deformation/fragmentation process characterized by flattening of the spherical drop leading to the formation of a bag bounded by a thick rim which eventually collapses to form smaller droplets. The present work seeks to advance the current understanding by comparing experimental evidence with theoretical predictions.

1. Introduction and Background

The disintegration of bulk fluid into smaller droplets, commonly referred to as atomization, finds diverse applications in industry. Atomization is broadly classified into two types: primary and secondary. Primary atomization refers to the initial breakup of a fluid jet or sheet into drops and occurs immediately after the liquid exits the injector orifice. On the other hand, secondary atomization occurs when the drops formed upon primary breakup undergo further fragmentation. The latter phenomenon is the focus of this study.

Previous studies [10,20,8,26,11,3,4,24,27] have reported experimental data acquired using three methods: shock tubes, drop towers and continuous jets. While each differs in terms of the manner in which aerodynamic forces are applied to drops, there is considerable agreement on the regimes of breakup involved.

Lane (1951)[16] was the first to observe the existence of multiple breakup regimes based on initial *We*, which he defined as

$$We = \frac{\rho_a U_0^2 d_0}{\sigma} \tag{1}$$

Here, ρ_a is the density of the ambient fluid, U_0 is the initial relative velocity between the drop and the surrounding gas, d_0 is the drop initial spherical diameter, and σ is the surface tension between air and drop. Whether the drops are inviscid is reflected by,

$$Oh = \frac{\mu_{liq}}{\sqrt{\rho_a \sigma d_0}} \tag{2}$$

Here, μ_{liq} is the dynamic viscosity of the liquid and other parameters are as defined in (1). Typically, $Oh < 0.1$ for inviscid drops.

There have been two comprehensive reviews of secondary breakup, the first by [19] and more recently by [9]. Based on them five important regimes are delineated and are shown in Fig. 1 in order of increasing *We*.

* Corresponding author: sojka@ecn.purdue.edu
† Presently at Sandia National Laboratories, Albuquerque, NM, U.S.A.

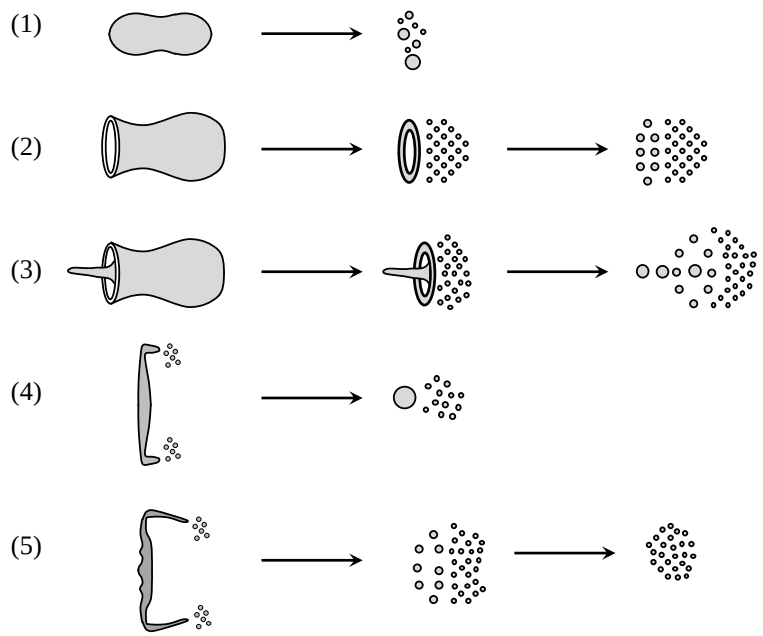

Fig 1: Five regimes of breakup for a low viscosity(inviscid) Newtonian drop in the presence of a horizontally flowing air stream as adapted from [19]

(1) Vibrational ($We \leq 11$)
(2) Bag Breakup (focus of present study) ($11 \leq We \leq 35$)
(3) Bag and stamen, or multi-mode ($35 \leq We \leq 80$)
(4) Sheet thinning, or shear stripping ($80 \leq We \leq 350$)
(5) Catastrophic ($We \leq 350$)

The objective of the present study is to analyze the bag breakup process in detail.

The study of bag breakup of a drop in air stream goes back at least to Lenard's [17] work in 1904. Bag breakup was reported by several researchers thereafter [10, 8, 3]. The various stages of the breakup process, as outlined by [7, 25] amongst others are shown in Fig 2. The drop evolves from a pancake/nearly oblate spheroidal structure to an approximately spherical bag attached to a toroidal rim.

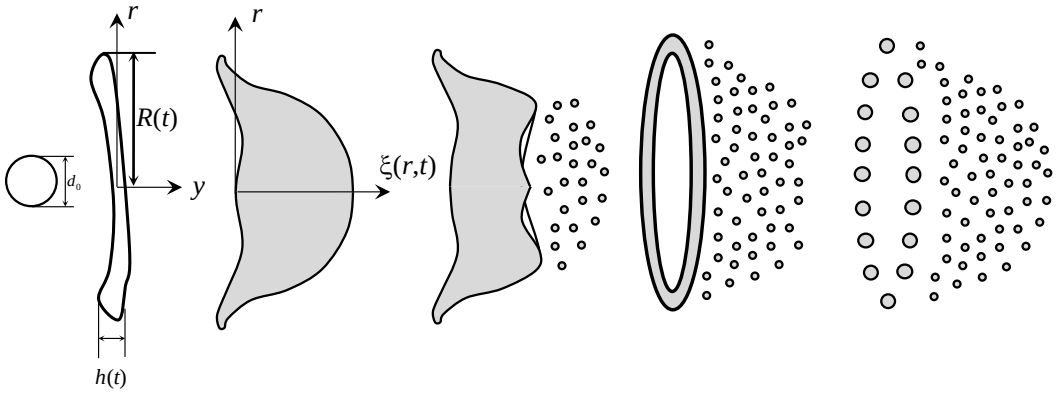

Fig 2: Stages of bag breakup

(1) Initial drop of diameter d_0 (2) Oblate spheroid stage (3) Bag growth
(4) Initiation of bag bursting (5) Complete bag fragmentation (6) Toroidal ring breakup

Various explanations have been put forth for the drop deformation process and it eventual bursting. Most researchers [15, 23, 1] have explained the entire drop deformation and bag burst process based upon on the formation of Rayleigh-Taylor waves whose wavelength is of the same order of magnitude as the drop. More recent-

ly [9] argued along similar lines ascribing breakup to RTP (Rayleigh-Tayor piercing). Except for work by [25] there does not seem to be predictions that describe the bag shape at various times and which compare well with experimental results.

In the context of liquid atomization, the regime boundary between the vibrational and bag breakup modes is particularly important because it marks the onset of guaranteed drop breakup [19]. An attempt has been made in this study to determine to this limit theoretically. [21,22] was the first to establish this boundary on the basis of analytical considerations, but their predictions were in agreement to only an order of magnitude [9]. In this study characteristic times, such as initiation time are also compared with experimental results.

2. Materials and Methods

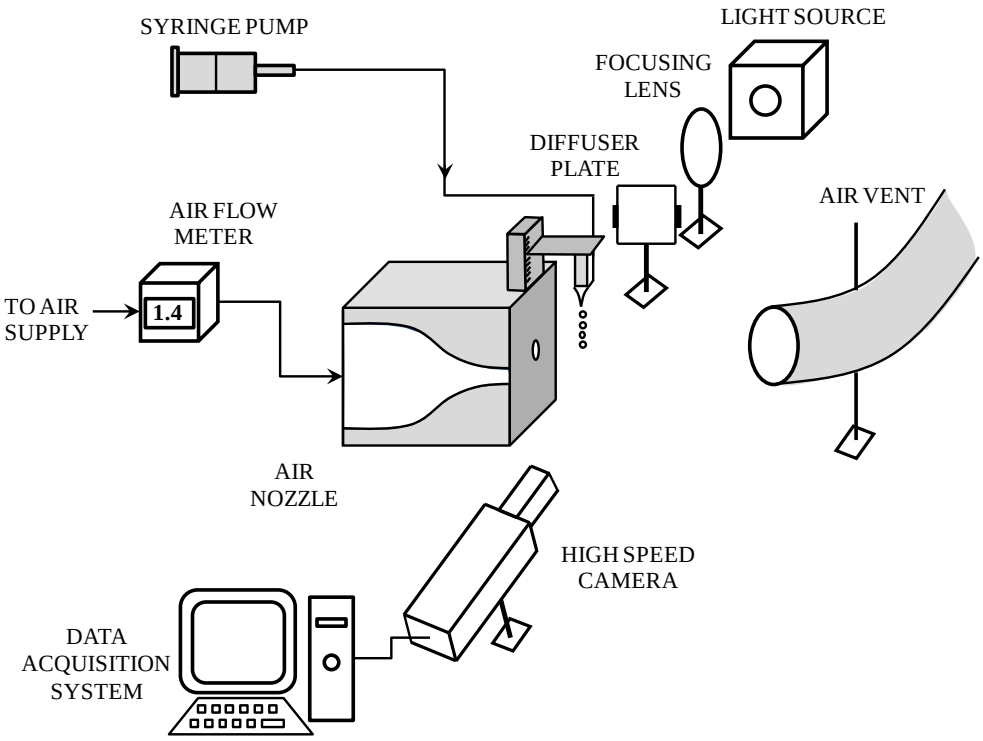

Fig 3: The experimental setup

The experimental setup is shown in Fig. 3. It consists of a drop generator, air flow system and high speed camera coupled to a data acquisition system.

The air flow system included an air supply line from the facility source, shutoff and needle valves, an air flow meter and a flow conditioning nozzle. The nozzle shape is such that the results obtained are comparable to those from continuous jet and shock tube experiments because the smoothly converging geometry minimizes boundary layer effects and therefore subjects the drops to a more spatially uniform step change in velocity.

A high speed imaging system is used to capture images of the drops as they fall into the air jet and fragment. It consists of a 1000 W Xe arc lamp used to produce a collimated beam that served as the illumination source, a plano-convex lens that focused the beam onto an opal glass diffuser, and a 105 mm Nikon lens attached to a Vision Research Phantom 7.1 high speed digital that allowed 800 × 600 pixel images to be recorded at 4700 frames per second. Measurements were made based on a set of three videos for each air flow rate condition.

Drop fragment sizes were measured using a dual-PDA(Phase Doppler Anemometer), a 112 mm unit from Dantec Dynamic having a 400 mm focal length transmitter lens and a 310 mm receiver lens, along with receiver mask C and a 200 μm slit. All photomultipliers (PMT) were operated at 1200 V.

Drop physical properties as obtained from [11] are shown below.

Liquid Physical Properties			
At 298 K	Density (kg/m^3)	Surface Tension(N/m)	Viscosity($Pa–S$)
Water	995	0.0733	8.93×10^{-4}
Ethyl Alcohol	788	0.0244	1.08×10^{-3}

3. Mathematical Model

Problem Formulation

We start with the formulation provided by [25]. Coordinate directions are from Fig 2.

3.1 *Air flow field*

Let, **U** = (U_r, U_y) be the velocities of air in the radial and streamwise directions. At this stage we are modeling between stages (1) and (2) in Fig. 2. Assuming the local air flow has the structure of a stagnation point, $U_y = -\gamma y$. The value of γ, the stretching rate, merges into that for a disc and a sphere at the appropriate limits.

In the inviscid, incompressible, quasi-steady assumption conservation of air momentum and mass give

$$\rho_a U_y \frac{\partial U_y}{\partial y} = -\frac{\partial p_a}{\partial y} \tag{3}$$

$$\rho_a U_r \frac{\partial U_r}{\partial r} = -\frac{\partial p_a}{\partial r} \tag{4}$$

$$r\frac{\partial U_y}{\partial y} + \frac{\partial (rU_r)}{\partial r} = 0 \tag{5}$$

From (3) we get $U_r = \frac{r\gamma}{2}$. Using (4) we can write,

$$p_l(r) = p_a(0) - \frac{\rho_a \gamma^2 r^2}{8} \tag{6}$$

where, $p_a(0) = \frac{\rho_a U^2}{2}$ the stagnation pressure at $r = y = 0$. (7)

The liquid pressure is, $p_l(r) = p_a(r) + \sigma\kappa$ which at $r << R(t)$ (8)

takes the form, $p_l(R) = p_a(0) - \frac{\rho_a \gamma^2 R^2}{8} + \frac{2\sigma}{h}$ (9)

3.2 *Liquid flow field*

For the deforming liquid we solve the Euler equations to get

$$\rho_l \left(\frac{\partial u}{\partial t} + u\frac{\partial u}{\partial r} \right) = -\frac{\partial p}{\partial r} \tag{10}$$

$$r\frac{\partial h}{\partial t} + u\frac{\partial (ruh)}{\partial r} = 0 \tag{11}$$

u (r,t) is the velocity field inside the drop which from (11) and global mass conservation

$$h(t) = \frac{d_0^3}{6R^2(t)} \tag{12}$$

yields a velocity field given by, $u(r,t) = \frac{r\dot{R}}{R}$ (13)

Integrating (10) between $r = 0$ and $r = R(t)$, and non-dimensionalizing the resulting equation, we get

$$\frac{\ddot{R}}{R} = \frac{1}{\tau^2}\left(1 - \frac{We_{cr}}{We}\right) \tag{14}$$

We is as defined in (1) and τ is the characteristic time scale for breakup, given by

$$\tau = \frac{\alpha d_0}{U}\sqrt{\frac{\rho_l}{\rho_a}} \tag{15}$$

Bearing in mind that [25] quantify the change in drop topology on a time scale typical of drops falling vertically in quiescent air, we note our physical situation occurs at a different time scale, so we multiply the right hand side of Equation (15) by 2 so as to give $We_{cr} = 12$ as reported in earlier studies [19,13]. α, signifies this adjustment and can be viewed as a model constant.

Since, (14) is a second order ordinary differential equation, the solutions growing with time correspond to $We > We_{cr}$ where We_{cr} marks the transition from the drop oscillatory to the bag breakup stage. The consistency of this value with earlier observations is summarised by [23]; it depends on γ and can be set to match these results. An accurate formulation of the evolving air flow field can be made but is superfluous in this case where we are within limits of good accuracy.

3.3 *Oblate spheroid stage, h(t)*

From (11) , and setting $\tilde{t} = t\frac{\dot{R}}{R}$ we obtain

$$\frac{\partial h}{\partial \tilde{t}} + r\frac{\partial h}{\partial r} + 2h = 0 \tag{16}$$

Equation (16) yields an asymptotic solution independent of *r*

$$h(t) \sim d_0 e^{-\frac{2t}{\tau}} \tag{17}$$

3.4 *Bag Growth, $\xi(r,t)$*

We can write the following force balance in the slender slope approximation for bag growth $\left|\frac{\partial \xi(r,t)}{\partial r}\right| << 1$

$$\ddot{\xi}(r,t) = \frac{p_l(r)}{\rho_l h(t)} \tag{18}$$

Using (18) with the initial condition, $\dot{\xi}(r, t=0) = 0$

$$\xi(r,t) = \frac{p_l(r)}{\rho d_0}\frac{\tau^2}{4}\left(e^{\frac{2t}{\tau}} - \frac{2t}{\tau} - 1\right) \tag{19}$$

3.5 *Drop Size Estimates*

The ring breaks owing to capillary instability and the dispersion relation is given by [7]

$$\omega^2 = Ak^2\left(\frac{R_0}{r_0}\right)^{1/2} - Bk^2\left(\frac{r_0}{R_0}\right)^{1/2} \tag{20}$$

where, *A* and *B* are constants. Here, R_0 and r_0 are the outer and inner radii, *k* is the wavenumber and ω the corresponding growth rate. The maximum dimensionless wavelength here varies as [7]

$$\beta = 0.707\sqrt{\frac{R_0}{r_0}} \tag{21}$$

By equating drop volume to the volume of a column of one wavelength we arrive at an estimate for d_{rim}.

The bag bursts due to the Rayleigh-Taylor instability as a result of the accelerated movement of the hemispherical liquid film in a direction perpendicular to the flow [2, 25]. These are seen as undulations on the bag having a wavelength dictated by such instability. We have not attempted such an analysis, so instead we use the following expressions to approximate the smaller drop sizes,

$$V_{total} = V_{ring} + V_{bag} \tag{22}$$

Here, t is the time at which the Rayleigh-Taylor instability becomes dominant. Calculating the bag thickness by assuming it to be a hemispherical shell, we can estimate its thickness. This thickness is then taken to be the fragment drop size d_{frag}.

$$V_{ring} = \frac{\pi^2 h(t)\left[2R(t) - h(t)\right]}{4}, \; V_{total} = \frac{\pi d_0^3}{6} \tag{23}$$

$$d_{frag} = R(t) - 1.1447\left[\frac{d_0^3}{6} - \left(\frac{\pi h(t)^2}{2}\right)\left(R(t) - \frac{h(t)}{2}\right)\right]^{1/3} \tag{24}$$

The value $R(t)$ is given by equation (12) and corresponds to asymptotic solution of $h(t)$ as obtained in equation (17).

4. Results and Discussion

Fig. 4 depicts bag breakup of a water and ethanol drop. Salient features include flattening, bag formation and bursting. Bag bursting can almost certainly be attributed to a Rayleigh-Taylor mechanism, as evident by the waves being formed in Fig 4. (*iv*). Topological changes shown in (*v*) and (*vi*) have been studied by other investigators [14, 15, 23, 24].

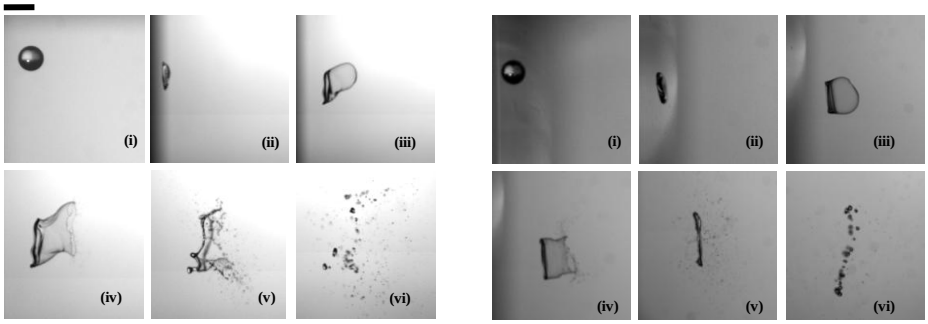

Fig 4: Deformation of a liquid drop of D.I. water (*left*) and ethanol (*right*). *We* ~ 27
Scale corresponds 4 mm

4.1 *Initiation time* (T_{ini})

Initiation time, T_{ini}, is defined as that required for a drop to deform beyond the oblate spheroidal shape. For example, the initiation time for bag breakup would be that at first sign of bag formation.

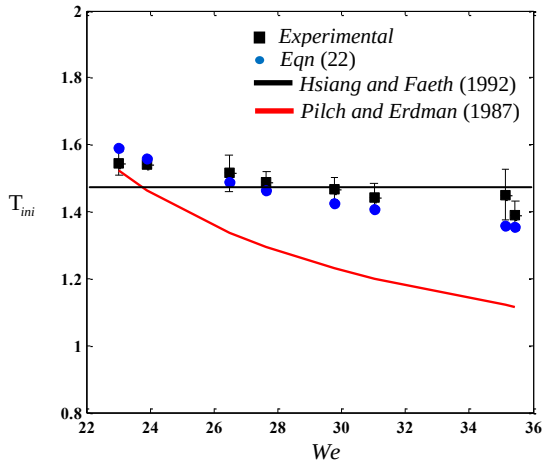

Fig 5: Comparison of initiation time as found by equation (25) with previous literature [11,19]

In Fig 5 we have used equation (14) to get equation (25) and plotted the values thus obtained alongside the corresponding experimental data.

$$T_{ini} = Cosh^{-1}\left(\frac{R_{final}}{R_0}\right)\frac{\tau}{\sqrt{\left(1-\frac{We_{cr}}{We}\right)}} \tag{25}$$

Other models such TAB (Taylor Analogy Breakup), ETAB (Enhanced TAB Model) and NLTAB concur with the experimental results, as does the correlation from [19]. Hence, we make our comparisons with the experimental result directly. Note that the modelling at this stage does not seek to improve accuracy of these existing models as they are found to work well. Instead, we focus on extending this modelling to better understand the bag breakup phenomena. This shall be described in the following sections.

4.2 *Bag growth*

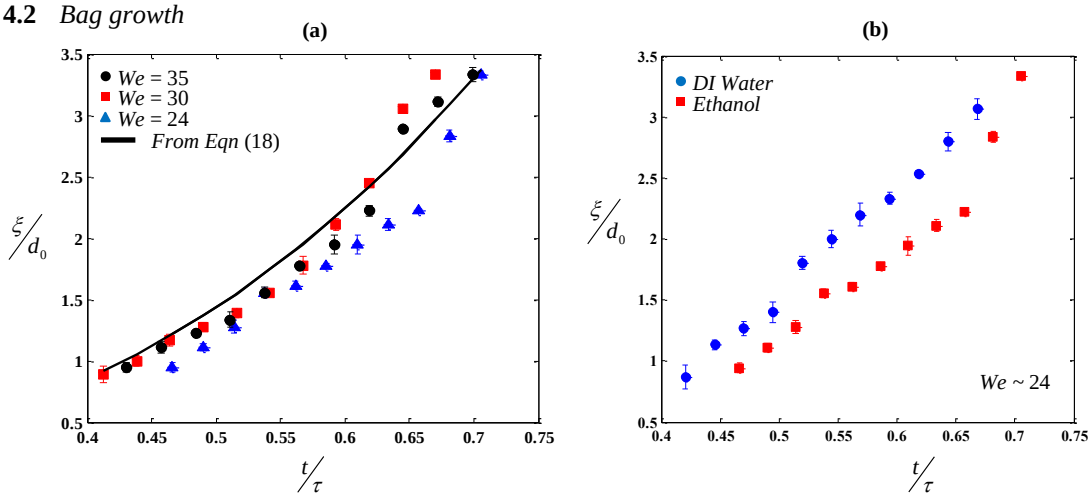

Fig 6 (a): Maximum ethanol bag size at various times and comparison with predictions.
(b) Ethanol and water bag sizes for *We* ~ 24

For one liquid, in this case ethanol, experimental bag growth is not dependent on *We*. This finding is consistent with model predictions from equation (18). A comparison between water and ethanol bag sizes shows an increase for water compared to ethanol. The model may not capture this difference since it does not include viscous effects.

4.3 *Drop Size Distribution*

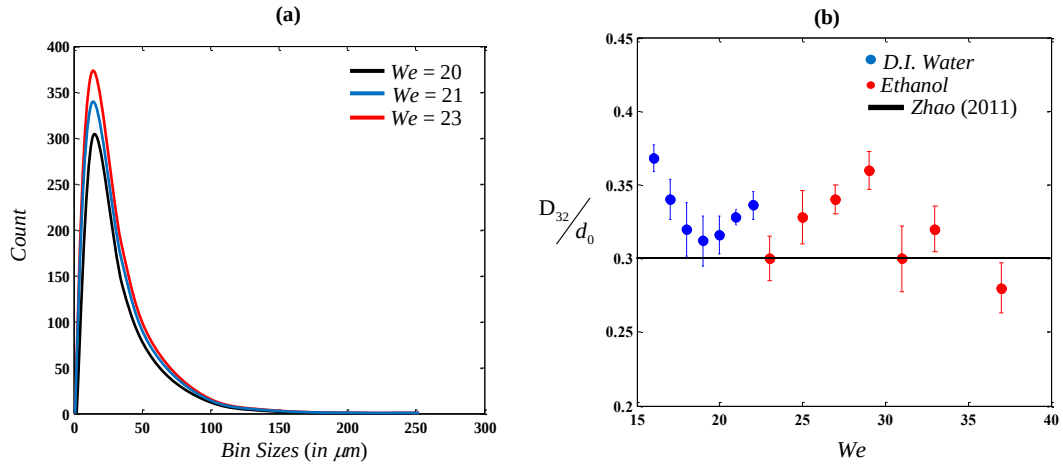

Fig 7(a) : Number density distribution showing variation in drop size distribution (experimental fragment size data fitted with a smoothing curve) (b) Variation of experimental D_{32} with *We* for Ethanol and D.I. Water.

Measured fragment size distribution and characteristic diameter data are shown in Fig. 7. Sample sizes are 8000 drops. The expected bi-modal distribution was not observed in the experimental runs because the probability of larger drops was insignificant for these tests. Larger data sets will be collected in the future.

The dimensionless D_{32} measurements as shown in Fig 7(b) show no particular dependence on *We*, but were consistent with the average value of ~ 0.3 reported by [27]. The rim and bag fragment diameters, as estimated from equations (21) and (24), serve as bounds for the observed values. These were found to be approximately 150 and 50 μm for fragments formed from the rim and bag, respectively. They correspond to 0.6 and 0.2 in non-dimensional terms on the Fig. 7(b) vertical axis.

6. Summary and Conclusions

This study reports new experimental data on drops undergoing fragmentation in the bag breakup regime. An analytical model is developed to highlight some of the important aspects of the bag evolution process. It characterises the changing shape of the bag for inviscid liquids. Model predictions are within the scatter of the measurement values. Dimensionless maximum bag growth is within ± 25% of experimental data. Furthermore, theoretical predictions show no dependence on *We*, consistent with experimental findings. Finally, the model correctly predicts We_{cr}, which marks the transition from the vibrational to the bag process.

A slight increase in bag size for water versus ethanol is attributed to higher viscosity of ethanol. This effect can not be predicted by our inviscid model. In addition, measured non-dimensional D_{32} had a mean value 0.32 over the range of *We* measured, with essentially no quantitative dependence between the two, consistent with previous findings. Finally, although [25] observed a sharp rise in bag sizes at longer times, no evidence of such behaviour is found in our experimental runs. This may be due to different loading conditions which in case of [25] was a situation similar to a drop tower in contrast to our case where the drop is injected into a horizontal jet stream.

The model may be further improved by more accurately resolving the air flow field around the moving drop. It may also be improved by using a Rayleigh-Taylor instability analysis to compute bag bursting behavior, instead of the estimates employed here. That analysis is underway. Regardless, the results presented here clarify the underlying mechanisms of bag formation and its eventual bursting.

7. References

[1] Arcoumanis C, Whitelaw DS, Whitelaw JH (1996) *Atomization and Sprays*. 6 :245–256
[2] Bremond C, Villermaux V (2005), *Journal of Fluid Mechanics.* 524:121–130.
[3] Chou WH, Faeth GM (1998) *International Journal of Multiphase Flow*. 24(6): 889-912.
[4] Dai Z, Faeth GM (2001) *International Journal of Multiphase Flow*. 27(2): 217-236.
[5] Dodd K N (1960), *Journal of Fluid Mechanics.* 9(2): 175-182
[6] Faeth GM, Hsiang LP, Wu PK (1995) *International Journal of Multiphase Flow*. 21: 99-127.
[7] Gast, L,(1991) *PhD* Thesis, Rutgers, The State University of New Jersey
[8] Gelfand BE (1996) *Progress in Energy and Combustion Science*. 22(3): 201-265.
[9] Guildenbecher D, López-Rivera C, Sojka P (2009) *Experiments in Fluids*. 46(3): 371-402.
[10] Hinze HO (1955) *AIChE Journal*. 1(3): 289-295.
[11] Hsiang LP, Faeth GM (1992) *International Journal of Multiphase Flow*. 18(5): 635-652.
[12] Hsiang LP, Faeth GM (1993) *International Journal of Multiphase Flow*. 19(5): 721-735.153
[13] Hsiang LP, Faeth GM (1995) *International Journal of Multiphase Flow*. 21(4): 545-560.
[14] Joseph DD, Beavers GS, Funada T (2002) *Journal of Fluid Mechanics*. 453: 109-132.
[15] Joseph DD, Belanger J, Beavers GS (1999) *International Journal of Multiphase Flow*.25 (6-7): 1263-1303.
[16] Lane W, (1951) *Ind. Eng. Chem. Res.* 43: 1312-1317.
[17] Lenard P(1904), *Meteor Z.* 24:249-262
[18] Lopez-Rivera and Sojka (2008) 22nd *ILASS Europe, Como Lake, Italy.*
[19] Pilch M, Erdman CA (1987) *International Journal of Multiphase Flow*. 13(6): 741-757.
[20] Ranger AA, Nicholls JA (1969) *AIAA Journal*. 7(2): 285-290.
[21] Tarnogrodzki A (1993) *International Journal of Multiphase Flow*. 19(3): 329-336.158
[22] Tarnogrodzki A (2001) *International Journal of Mechanical Sciences*.43(4):883-893
[23] Theofanous TG, Li GJ, Dinh TN (2004) *Journal of Fluids Engineering*. 126(4): 516-527.
[24] Theofanous TG(2011) *Annual Review of Fluid Mechanics.* 43:661–90
[25] Villermaux E., Bossa B (2009) *Nature Physics*. 5: 697 - 702
[26] Wierzba A, Takayama K (1988) *AIAA Journal*. 26(11): 1329-1335.
[27] Zhao H., Liu H.F., Xu J.L., and Li W.F(2011) *Ind. Eng. Chem. Res.*50: 9767–9773